JMEPEG (2008) 17:674–681
DOI: 10.1007/s11665-008-9219-3

1059-9495/$19.00

Surface Characterization of 7075-T73 Aluminum Exposed to Anodizing Pretreatment Solutions

Terence P. Savas and James C. Earthman

(Submitted January 16, 2008)

Localized corrosion damage in Type 7075-T73 aluminum alloy was investigated for various anodizing pretreatment solutions. The postexposure surface corrosion was characterized by use of scanning electron microscopy (SEM) examination. In addition, SEM and energy dispersive spectroscopy (EDS) were used for second-phase (constituent) particle identification for those found to induce pitting corrosion during solution exposure. The pitting mechanisms were identified as circumferential where the particles are noble with respect to the matrix phase and by selective dissolution where they are anodic. The designated category-1 degreasing and category-2 inhibited alkaline solutions did not initiate localized corrosion after 1200 s exposures. However, the category-3 high-pH NaOH and category-4 low-pH HNO_3 based solutions were found to initiate pitting attack, with the NaOH being significantly more aggressive. It was hypothesized that if the pits initiating during the pretreatment exposures were beyond a threshold size, on the order of 10-20 μm, a higher current density existed at these locations during subsequent electrochemical processes, thus resulting in larger and deeper pit structures. These surface defects are of primary concern with respect to accelerated fatigue crack nucleation. For smaller pits, on the order of 1-5 μm, the anodic process had a smoothing affect where the film growth tended to passivate the pits.

Keywords aluminum, anodizing, caustic etch, deoxidizer solutions, fatigue crack initiation, pitting corrosion, pretreatment solutions, scanning electron microscopy, 7075-T73

1. Introduction

Anodic coatings are used extensively for in-service corrosion protection of hydraulic manifolds and similar flight control actuator components fabricated from high-strength aluminum alloys. The most common processes used to produce these coatings are defined as Type-I chromic acid, Type-II sulfuric acid, and Type-IIB thin sulfuric acid anodizing (Ref 1). Specific details of the respective coatings including anodizing bath process parameters, corrosion resistance, wear resistance, and thickness ranges can be found in various publications (Ref 2-4). While these coatings were developed to extend service life, they have been found to be deleterious for certain alloys and heat treatments. Specifically, localized corrosion occurring during pretreatment solution exposure creates pit structures that have been identified as a cause for accelerated crack nucleation during subsequent fatigue loading (Ref 5, 6). Because component failure can be greatly accelerated by the presence of these surface defects, a comprehensive understanding of these pretreatment corrosion mechanisms is therefore of scientific interest and technological importance.

Terence P. Savas, Control Systems Division, Parker Hannifin Corporation, Aerospace Group, Irvine, CA 92618-1898; and **James C. Earthman**, Department of Chemical Engineering and Materials Science, University of California Irvine, Irvine, CA 92697-2575. Contact e-mail: tsavas@parker.com.

Passive film breakdown in alloyed aluminum will occur predominantly at constituent particle locations or grain boundaries that have lower concentrations of aluminum and thus weaker passive films (Ref 7, 8). In the present article, the term 'constituent particles' is used to designate the insoluble, undissolved, or precipitated coarse particles that are formed and distributed heterogeneously in aluminum alloys. They form from impurity elements, excess alloying elements, or improper heat treatment (Ref 9). During solution exposure, the differences in chemical potential between the particles and surrounding matrix promote corrosion reactions where charge and mass transfer can readily occur (Ref 10). In aluminum alloys, two main types of pit morphologies are observed (Ref 11), one type is designated as circumferential that appears as a ring of attack around a particle or colony of particles. This attack is mainly in the matrix phase and is ascribed to a local galvanic attack of the more active matrix by the more noble particles.

The second type of pit morphology is designated as selective dissolution. Pit structures of this type are typically deeper and may have remnants of the particle in them. This type of damage has also been referred to as particle fallout. A compilation of corrosion potentials have been reported by Buchheit for intermetallic phases in aluminum alloys (Ref 12). This study provides a comprehensive breakdown of the particle types and galvanic relationships among discrete microstructural elements and phases in aluminum alloys.

A recent investigation (Ref 9) by Wei et al. for particle-induced corrosion of 7075-T6 and 2024-T3 aluminum alloys indicated that the electrochemical characters of constituent particles are different and may be broadly divided into two groups. Particles that contain Al, Cu, and Mg tend to be anodic relative to the alloy matrix, while those that contain Al, Cu, Fe, and Mn tend to be cathodic relative to the matrix. Scanning electron microscopy (SEM) examinations suggested the anodic particles tended to dissolve preferentially, whereas cathodic

particles tended to promote dissolution of the neighboring matrix in 0.1 M NaCl solutions.

During a typical anodize process, a part may be subjected to over ten different process baths (including water rinse cycles) (Ref 3). It is therefore critical to understand the affect of each solution individually and the combined affects for multiple exposures. A proper pretreatment process is necessary to produce a chemically clean surface that is a precursor for a uniform and reliable anodic coating. The purpose of each solution type can be categorized as follows: (1) liquid or vapor degreasing, (2) nonetching alkaline cleaners, (3) high-pH etching (caustic) cleaners, (4) low-pH acid-based deoxidizers, (5) low-pH sulfuric and chromic acid (for the anodize process), and (6) sealing solutions.

The category-1 process removes oils and greases as well as solid dirt particles from the metal surfaces. Noninflammable chlorinated hydrocarbon solvents have historically been used for degreasing, the most common of which is trichloroethylene. More recently, environmental restrictions have been imposed on use of chlorinated solvents and they have been replaced with liquid degreasing (detergent) based solutions for the majority of applications. The process baths are normally agitated and maintained at a temperature range of 70-95 °C (160-200 °F). This degreasing process will not, however, produce a chemically clean (water-break-free) surface and is therefore supplemented by use of alkaline cleaners.

The category-2 alkaline cleaners are important in the case of aluminum since the highly alkaline solutions can readily cause pitting attack if not properly controlled with inhibitors. The function of the inhibitors is to provide a protective film which is formed by the reaction of the inhibitor with the aluminum or oxide surface, or, in the case of silicates, a mono-molecular layer of hydrated silica may be formed superficially (Ref 4). The actual cleaning agents are normally composed of mixtures of trisodium phosphate or sodium pyrophosphate with sodium metasilicate. The aqueous solutions are used at elevated temperatures, 70-95 °C (160-200 °F), sometimes with ultrasonic agitation. Surfactants are also used in these solutions as wetting agents and assist in immediate, uniform wetting, and thus more uniform cleaning. Typical exposure times for category-1 and -2 solutions are on the order of 600-900 s. Further details of the specific category-1 and -2 solutions can be found in Ref 13 and 14, respectively.

Consideration must also be given to the category-3 and -4 caustic etching and deoxidation solutions. The most common category-3 etching cleaner for aluminum is an aqueous solution of caustic soda, for example, NaOH, with or without additives. After removal of the grease and oils using the nonetching type cleaners, the high-pH caustic etch solutions are used to deoxidize the aluminum and will also tend to eliminate nicks, scratches, and other surface imperfections. The foremost purpose is to remove the natural oxide layer that readily forms on aluminum in the presence of oxygen. Removal of the oxide layer (often referred to as surface activation) allows for a more conductive surface thus facilitating subsequent electrochemical processes such as anodizing. In this reaction, NaOH reacts with the Al producing heat, hydrogen gas, and sodium aluminate ($NaAlO_2$). During the reaction of Al with NaOH, a scale of hydrated aluminum oxide ($Al(OH)_3$) forms. The complete reaction is represented by $2Al + 2NaOH + 2H_2O \rightarrow 2NaAlO_2 + 3H_2$ and $NaAlO_2 + 2H_2O \rightarrow Al(OH)_3 + NaOH$. A grey to black residual film is normally deposited on the surface during this process. These deposits usually consist of Mg, Zn, Fe, Cu, Si, and other alloying constituents in the aluminum that are not soluble in the NaOH solution. Caustic etch solutions are normally used in concentrations of 15-45 g/L (2-6 oz per gallon) at a working temperature range of 38-71 °C (100-160 °F) and a pH between 13.0 and 13.6 (Ref 15). Due to the aggressive nature of the caustic solutions, exposure times are typically limited a range between 30 and 120 s.

The category-4 low-pH nitric acid-based solutions previously noted are used effectively to remove the insoluble oxides, and are therefore referred to as deoxidizers. The most common type at the time of this publication, and the type investigated in the present study, consists of a $HNO_3 + Fe_2(SO_4)_3$ solution. Although the exact formulations are proprietary, the concentrates contain approximately 15-20% by weight nitric acid (HNO_3) and 40-60% by weight ferric sulfate ($Fe_2(SO_4)_3$) along with surfactants and wetting agents (Ref 16). The liquid concentrates are mixed with water to form 10-20% aqueous solutions at a working temperature range of 10-38 °C (50-100 °F) and a pH between 0.8 and 1.0. Some deoxidizers are chromated; however, these are also being phased out due to environmental restrictions. Exposure times for the deoxidizers range in the order of 120-600 s.

The specific objectives for the present study were as follows: (1) characterization of the 7075-T73 hand forged billet microstructure with respect to grain boundary structure, constituent particle-size, composition, and distribution using metallographic, SEM, and energy dispersive spectroscopy (EDS) examinations, (2) perform individual exposure experiments with 7075 in the category 1-4 pretreatment solutions previously described (and combinations of solutions) to characterize the severity of resulting corrosion damage. This includes one sample going through a complete anodize cycle to better understand the affects of preexisting pit defects during the actual electrochemical process, (3) establish optimum conditions to minimize localized corrosion defects, and (4) set the groundwork for future electrochemical measurements in the pretreatment solutions of most interest as determined during this study.

2. Procedures

2.1 Experimental Material

The as-received material consisted of Type 7075-T73 hand forged billet (Ref 17) with a 0.152 m (6 in) square cross section and a length of 0.381 m (15 in). To obtain the 7075 in a stabilized (overaged) T73 temper condition, the billets were solution heat treated at 471 °C (880 °F) for 7 h, water quenched at room temperature, artificially aged for 6 h a 107 °C (225 °F), and stabilized for 8 h at 177 °C (350 °F). The stabilized temper condition reduces the strength by approximately 10% (as compared to the peak strength T6 temper), but increases the materials resistance to sensitization and subsequent stress corrosion cracking (SCC). The chemical composition and mechanical properties are provided in Tables 1 and 2, respectively, for the specific heat lot used in this study.

2.2 Microstructural Examinations

For the present study, trends in the size, distribution, and composition of the constituent particles are of particular interest. Particle identification was based on SEM and EDS

Table 1 Chemical composition (wt.%) for 7073-T73 alloy evaluated in the present study

Alloy type	Cu	Fe	Si	Mn	Mg	Zn	Cr	Ti	Zr	V	Al
7075	1.5	0.26	0.07	0.020	2.4	5.6	0.19	0.02	···	···	Bal

Table 2 Mechanical properties for 7075-T73 alloy evaluated in the present study

Alloy type	Grain direction	Yield strength, MPa (ksi)	Tensile strength, MPa (ksi)	% Elongation
7075-T73	Longitudinal	381.3 (55.3)	460.5 (66.8)	15
	Long transverse	368.9 (53.5)	449.5 (65.2)	12.5
	Short transverse	402.7 (58.4)	477.2 (69.2)	7

techniques. These data are presented for particles found to induce pitting corrosion during the exposure experiments. Figure 1(a) and (b) illustrates the polished and etched microstructure for alloy 7075-T73 for the L and ST grain directions, respectively, with important constituent particles identified. The postexposure SEM surface examinations were taken on a plane normal to the ST grain direction each at the same magnification to aid in the comparisons. The particles of interest are temporarily designated as 7075-A and 7075-B. Attempts were not made to predict the actual crystal structure and stoichiometry of the particles, but rather measure the peak intensity of the alloying elements relative to the overall composition.

2.3 Exposure Experiments

The corrosion coupons were extracted from the center portion of the aluminum billet with length, height, and thickness dimensions of 10 cm × 2.5 cm × 0.50 cm (4 in × 1 in × 0.20 in). The coupons contained a drilled hole on one end that was used for wire retention during solution exposure. After final machining the coupons were polished with 600-grit emery paper. The coupons were then ultrasonically cleaned in a mild soap solution, air-dried, and stored in a desiccator prior to exposure. Table 3 outlines the processing sequence for the samples (herein designated S1-S8) and includes the solution types, concentrations, temperatures, and exposure times. In all cases, the solutions were agitated by mechanical methods. All water rinse cycles and processing solutions utilized de-ionized (DI) water.

2.4 Quantitative Analysis

To quantify the pit sizes and distributions; digital image analysis was used, along with metallographic cross sectioning. For the present study, image analysis was conducted for samples exposed to the caustic etch solution for 120 s (sample S4) and for the deoxidation solution for 600 and 1200 s exposures (samples S5 and S8). This technique requires converting grey-scale SEM micrographs of the corroded surfaces into black and white binary images, and then digitizing the image. The image analysis software then provides various size and distribution parameters associated with the binary image features. These data were then used along with statistical analyses to quantify the corrosion damage associated with each solution type. Figure 2 shows a typical binary image from sample (S8) exposed to the deoxidation solution for

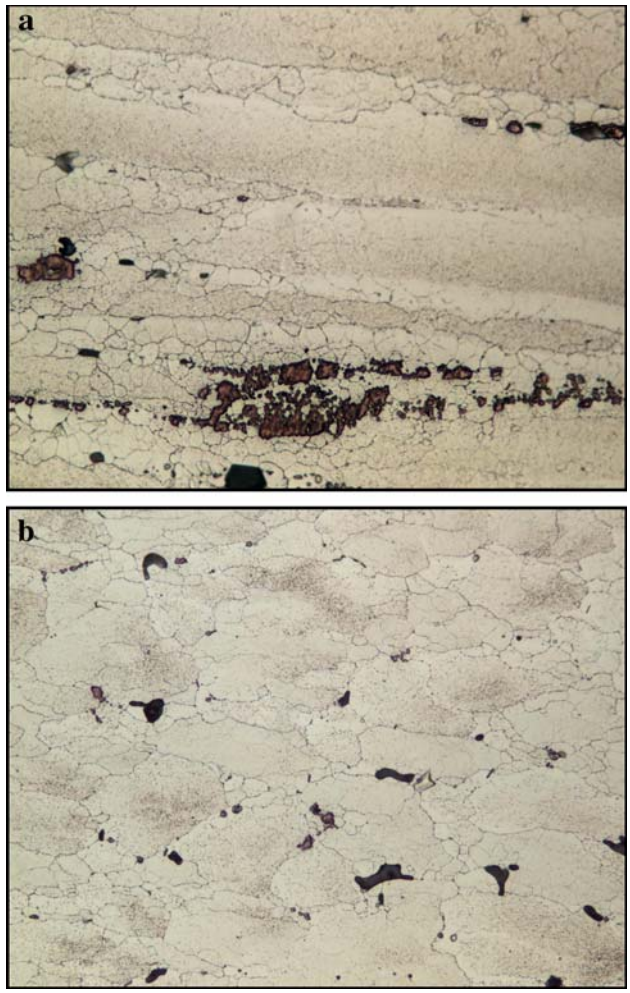

Fig. 1 (a) Microstructure of 7075-T73 Al alloy for longitudinal (*rolling*) grain direction with particles of interest designated 7075-A and 7075-B (500×). (b) Microstructure of 7075-T73 Al alloy for short-transverse grain direction with particles of interest designated 7075-A and 7075-B (500×)

1200 s. To quantify localized corrosion using this technique, the pit diameters and pit areas are commonly computed. If the feature shape is not a perfect circle, the software reports the average length of the diameters measured at two-degree (orthogonal angle) intervals joining two outline points and passing through the centroid.

3. Results

Figures 3 and 4 include SEM images of particles of type 7075-A and 7075-B. Figure 5 shows the EDS spectra for the overall alloy composition while Figs. 6 and 7 show the EDS spectra for the 7075-A and 7075-B particle compositions, respectively. The EDS spectra for the overall structure show peaks for the primary alloying elements in accordance with Table 1. The particle type designated as 7075-A showed elemental peaks for Fe and Cu while that for 7075-B showed peaks for Fe, Mg, and Si. The irregular shape and random distribution of the particles makes it difficult to characterize

Table 3 Surface process sequence for samples designated S1-S8

Solution Type/ Temperature	Category	S1	S2	S3	S4	S5	S6	S7	S8
Water Rinse/ 22ºC (72ºF)	—	120 s							
Liquid Degreaser/ 71ºC (160ºF) [13]	1 (A)		600 s					600 s	
Water Rinse/ 22ºC (72ºF)	—		120 s					120 s	
Alkaline Cleaner 71ºC (160ºF) [14]	2 (A)			600 s				600 s	
Water Rinse/ 22ºC (72ºF)	—			120 s				120	
Caustic Etch 71ºC (160ºF) [15]	3 (B)				120 s		120 s	120 s	
Water Rinse/ 22ºC (72ºF)	—				120 s		120 s	120 s	
Deoxidizer/ 22ºC (72ºF) [16]	4 (C)					600 s	120 s	120 s	1200 s
Water Rinse/ 22ºC (72ºF)	—					120 s	120 s	120 s	120 s
Type-II Anodize [1] 22ºC (72ºF)	5 (D)							1800 s	
Water Rinse/ 22ºC (72ºF)	—							120 s	
Seal/DI Water 93ºC (200ºF)	6							900 s	

(A) Solutions prepared as a 10% aqueous solution of liquid concentrate
(B) Solution prepared by mixing 30 g/L NaOH (solid granulated form)
(C) Solution prepared as a 10% aqueous solution of HNO_3 + $Fe_2(SO_4)_3$ liquid concentrate
(D) Solution prepared as 15% aqueous solution of sulfuric acid (H_2SO_4) and processed in accordance with (Ref 1)

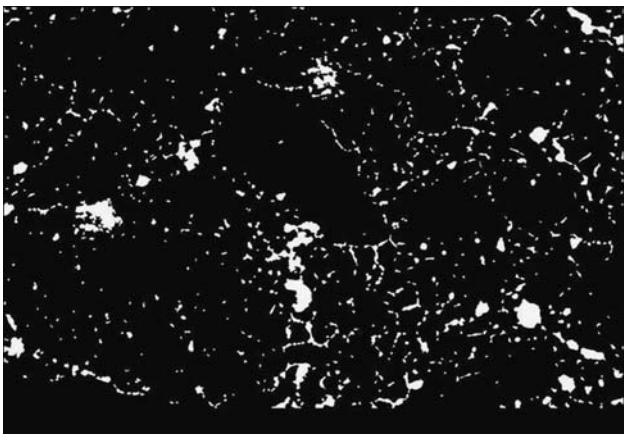

Fig. 2 Image analysis results for 7075-T73 after 1200 s exposure to a 10% solution of HNO_3 + $Fe_2(SO_4)_3$ concentrate at room temperature (500×)

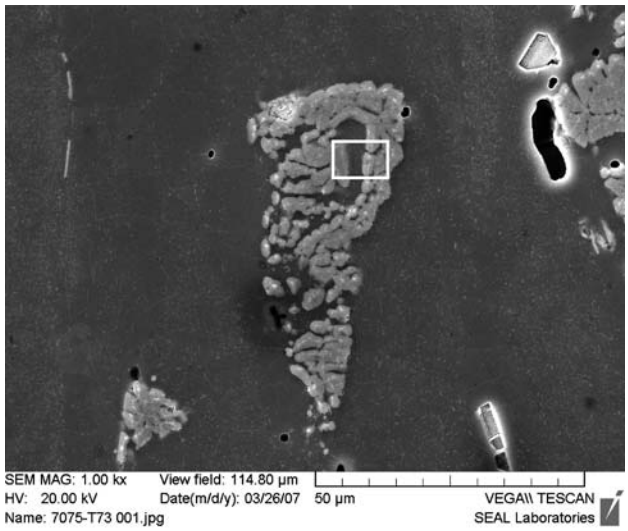

Fig. 3 SEM image of particle type designated 7075-A per Fig. 1 (1000×)

their size although their dimensions can be estimated from the micrographs. In general, the particle sizes were on the order of 10-50 µm.

The category-1 degreasing and category-2 inhibited (non-etching) alkaline solutions did not initiate localized corrosion. Figure 8 shows the as-machined surface with a single isolated micro-pit present. Figure 9 illustrates the surface corrosion created with a 120 s exposure to the NaOH solution (sample S4).

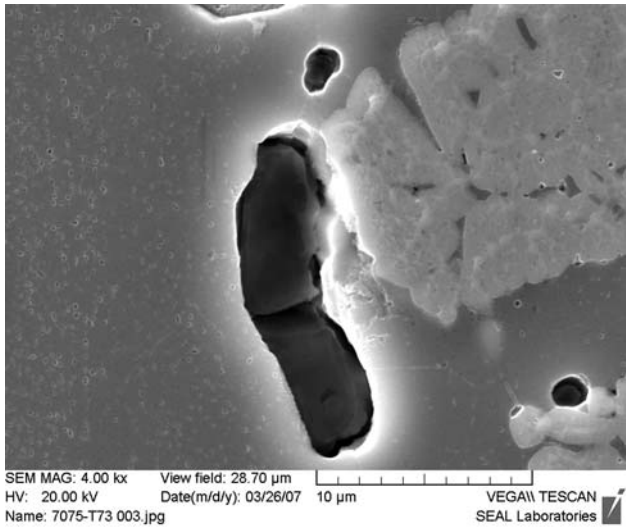

Fig. 4 SEM image of particle type designated 7075-B per Fig. 1 (4000×)

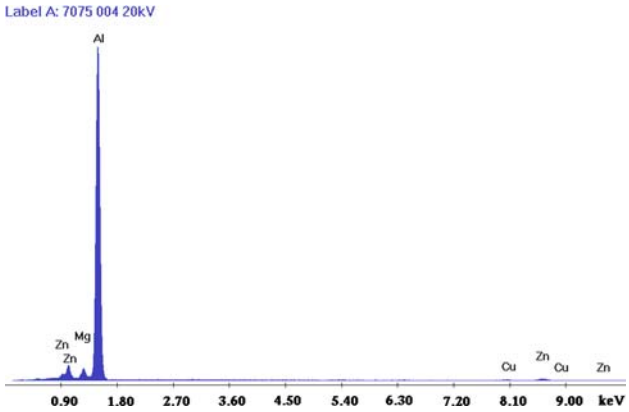

Fig. 5 EDS spectra for overall 7075 composition

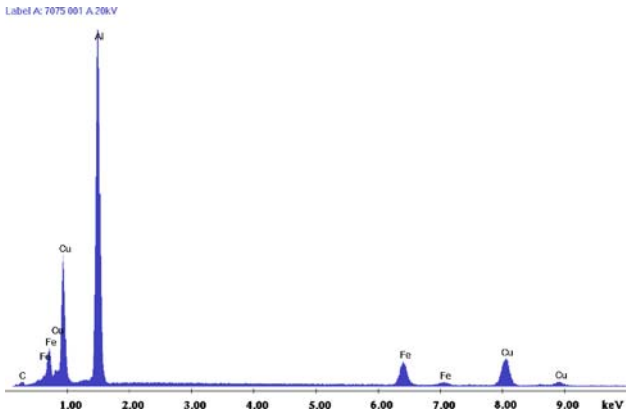

Fig. 6 EDS spectra for a typical particle designated 7075-A within the white box in Fig. 4

The cracked appearance is a layer of residual metal-oxide. As previously discussed, these deposits consist of Mg, Zn, Fe, Cu, Si, and other alloying constituents in the aluminum that are not soluble in the NaOH solution.

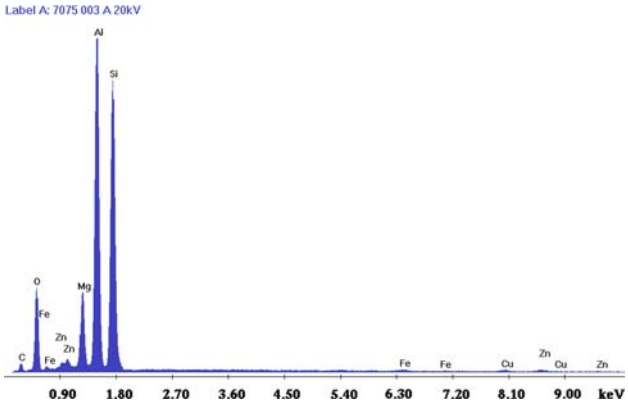

Fig. 7 EDS spectra for a typical particle of type 7075-B within the white box in Fig. 5

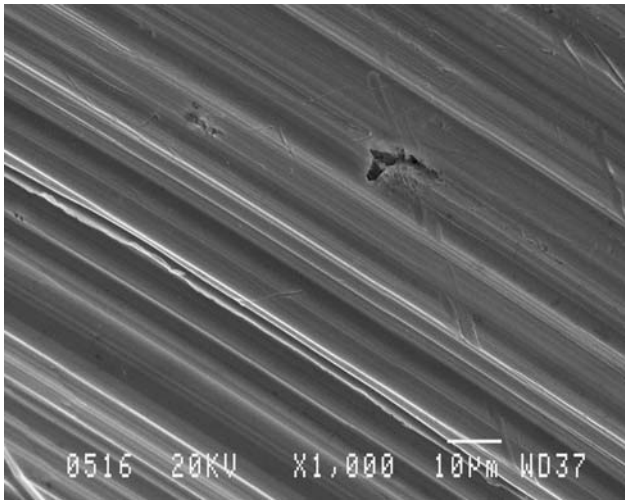

Fig. 8 As-machined surface of sample (S1) exposed to water rinse, note single isolated micropit (1000×)

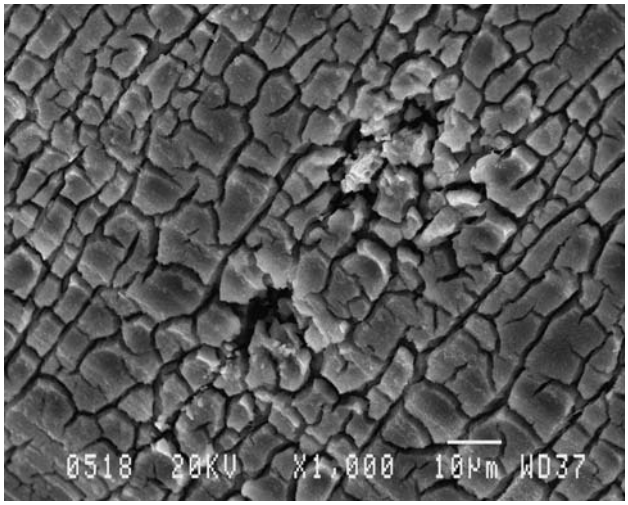

Fig. 9 Surface appearance of sample (S4) after exposure to 30 g/L NaOH solution at 71 °C (160 °F) for 120 s. Note cracked appearance of residual metal oxide film (1000×)

The same surface after removal of the undissolved oxides using ultrasonic agitation in a mild soap solution is illustrated in Fig. 10. The surface, in this case, shows general attack and round spherical-shaped pit structures at constituent particle locations. There were minor amounts of particle remnants within the pit structures. The caustic etch caused severe pitting attack with only 120 s exposure.

Figure 11 illustrates the surface corrosion after a 600 s exposure to a 10% aqueous solution of HNO_3 + $Fe_2(SO_4)_3$ concentrate at room temperature (sample S5). The 600 s was to represent a worst-case exposure time used in practice. Corrosion pits were not detected when exposure times were limited 60-120 s for this solution. Figure 12 shows a sample subjected to 120 s of caustic etch followed by 120 s exposure to the deoxidizer (sample S6). This shows the deoxidizer is highly effective in removing the residual metal oxides, but also creates additional pitting damage, for example, at the bottom of the spherical pits that resulted from the initial caustic etch.

The low-pH deoxidizer solution was less aggressive than the high-pH caustic solution. Figures 13 and 14 illustrate probability plots that were generated using the image analysis data. The best-fit straight line was achieved with a three-paramater lognormal distribution. For this type of distribution, the scale factor listed on the plot must be added to *x*-axis value to obtain the actual pit size. The following can be observed from these data: (1) the average pit diameter was approximately 1 and 7 μm for deoxidation and caustic solutions, respectively. (2) The largest pit diameter was approximately 10 μm (for 600 s exposure) and 37 μm for deoxidation and caustic solutions, respectively, and (3) the caustic solution created a significantly higher population of pits beyond the threshold critical size of 10 μm diameter. However, the pits that initiated in the deoxidizer solution were deeper and had more jagged edges as compared to the caustic solution where they were semispherical with smoother edges. Additionally, for the deoxidation solution, the particle remnants were largely left intact within the pits. On the basis of metallographic cross sections

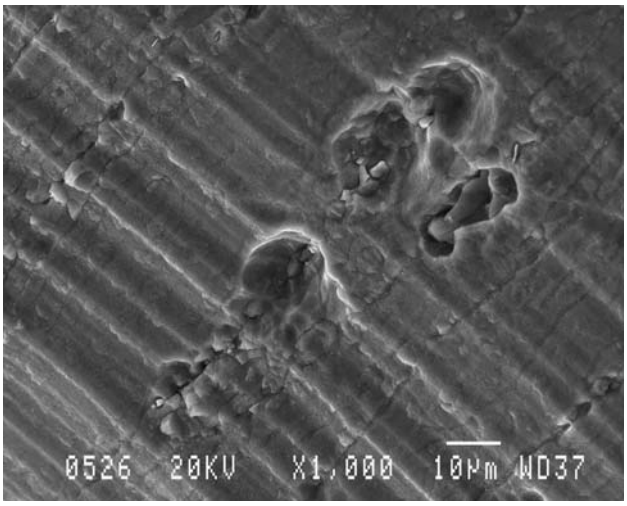

Fig. 10 Same surface shown in Fig. 9 after ultrasonic agitation in mild soap solution. Note general attack and semispherical shaped pits on the order of 10-20 μm in diameter (1000×)

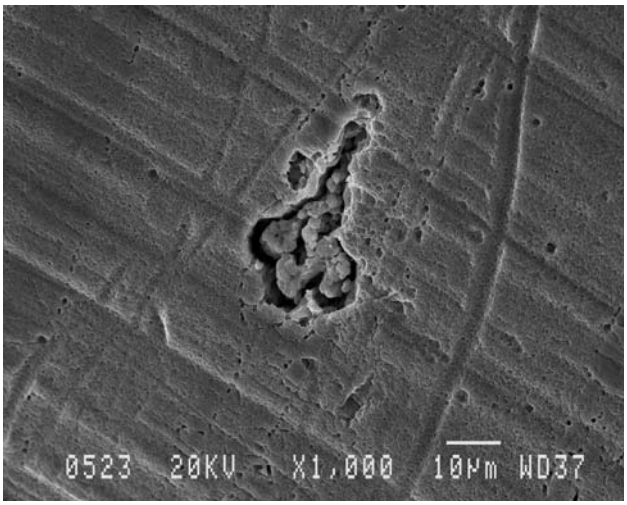

Fig. 11 Surface appearance for sample (S5) after 600 s exposure to 10% aqueous solution of HNO_3 + $Fe_2(SO_4)_3$ concentrate at room temperature. Note typical pit structure with jagged edges and particle remnants within the pit (1000×)

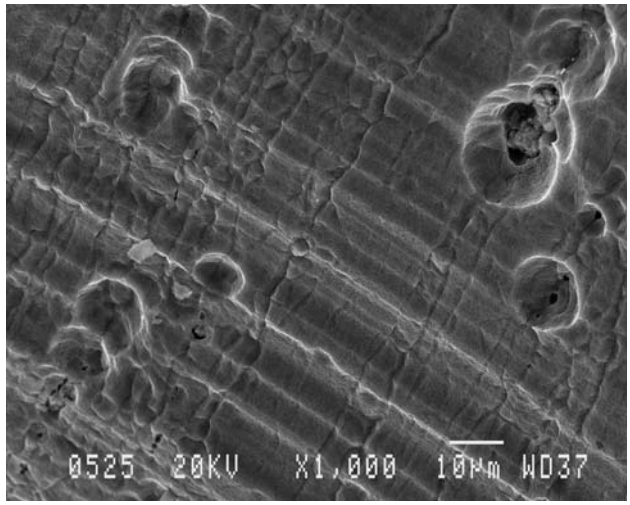

Fig. 12 Surface appearance for sample (S6) after 120 s exposure to 30 g/L NaOH solution at 71 °C (160 °F) followed by 120 exposure to 10% solution of HNO_3 + $Fe_2(SO_4)_3$ concentrate at room temperature (1000×)

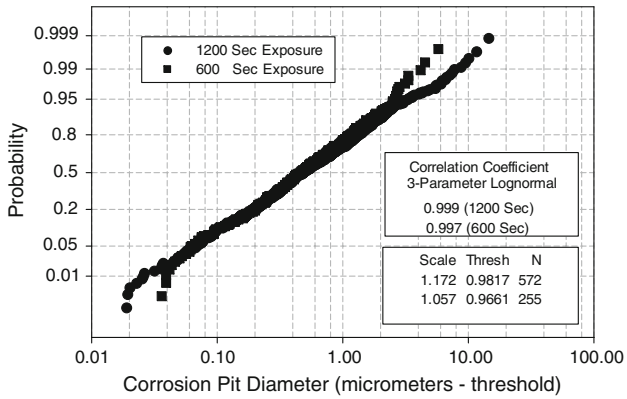

Fig. 13 Probability plot for three-paramater lognormal distribution of corrosion pit diameters for samples exposed to 10% aqueous solution of HNO_3 + $Fe_2(SO_4)_3$ concentrate for 600 and 1200 s durations

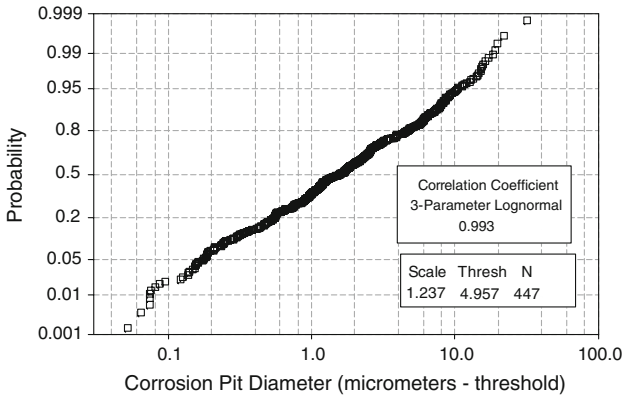

Fig. 14 Probability plot for three-paramater lognormal distribution of corrosion pit diameters for sample exposed to NaOH caustic etch for 120 s duration

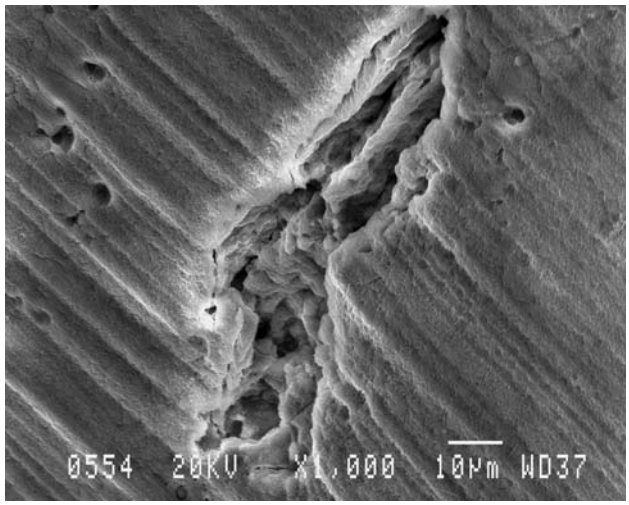

Fig. 15 Surface appearance for sample (S7) after exposure to complete sulfuric acid anodize cycle. Larger and deeper pit structures are observed as compared to that for the pretreatment solutions (1000×)

(not shown), the maximum and average pit depths were measured to be 9.1 and 4.1 µm for the deoxidizer solution, and 3.3 µm and 2.2 µm for the caustic solution, respectively.

It was of interest to examine the affects of preexisting pits that formed during the pretreatment process subsequent to the actual anodize process. Figure 15 shows a sample (S7) that was processed through a complete sulfuric acid anodize cycle. The anodic coating thickness in this case was measured to be 0.01 mm (0.0004 in) determined using eddy-current methods. Here the pits that initiated during the pretreatment cycle appeared to grow significantly in size and depths during the electrochemical anodize process. Evidence of the anodic coating is shown around the edge of the pits. It was discovered for relatively small pits, the anodic coating was actually able to grow over these pits and produce a smoother surface. We hypothesize that during the anodize process the current density is more highly concentrated at the surface defects, and if they are beyond a threshold size where the anodic film cannot grow over them, they will become larger and deeper (compare Figs. 11 and 15).

Examination of the surfaces after an overexposure was of specific interest for the deoxidizer solution. This condition may

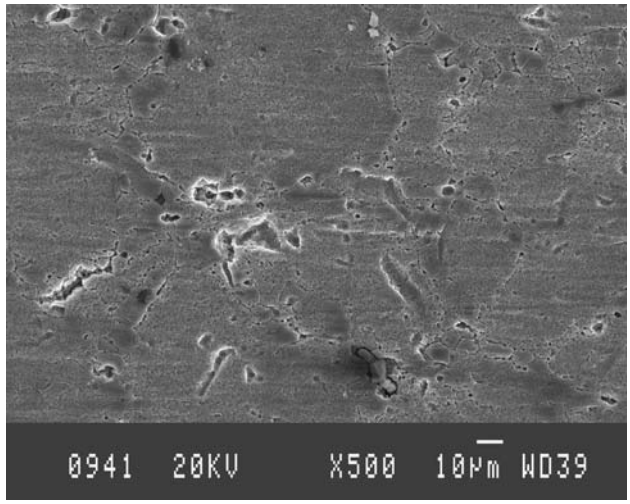

Fig. 16 Surface appearance for sample (S8) after 1200 s exposure to 10% aqueous solution of HNO_3 + $Fe_2(SO_4)_3$ concentrate at room temperature. Selective dissolution pitting mechanism for A-type particles and circumferential pitting mechanism for B-type particles is evident. Also note grain boundary attack for the longer exposure period (500×)

result, for example, due to poor process controls. Here the samples were exposed for 1200 s. This was also done to pinpoint pitting mechanisms associated with the two particle types. In this case, images are presented at 500× for a direct comparison to the as-polished structure depicted in Figs. 1(a) and (b). Figure 16 (sample S8) shows a pit originating at a 7075-A particle site (i.e. those with high concentrations of Fe and Cu). The pitting mechanism was identified to be selective dissolution where the particles are anodic with respect to the matrix phase. In contrast, the pitting mechanism was identified to be circumferential for the 7075-B particle sites (i.e. those with high concentrations of Fe, Mg, and Si) where the particles are cathodic with respect to the matrix phase. These findings were consistent with previous investigations of particle-induced corrosion of aluminum alloys (Ref 9).

A final observation is that the 7075 alloy exhibited significant intergranular attack after the 1200 s exposure. This was attributed to a high concentration of precipitate particles at the grain boundaries for this longer exposure time. This type of damage is particularly important with respect to SCC failure mechanisms (Ref 2).

4. Discussion and Conclusions

The present study focused on the influence of the following categories of pretreatment solutions on the corrosion behavior of 7075-T73 aluminum samples: (1) liquid degreasing, (2) non-etching alkaline cleaners, (3) etching (caustic) cleaners, (4) low-pH acid-based deoxidizers, and (5) low-pH sulfuric and chromic acid (for the anodize process). Samples were exposed to various solutions and combinations of solutions to better understand their corrosive affects with one sample going through a complete anodize process. It was concluded that the category-1 and -2 solutions did not cause any corrosion damage while the category-3 and -4 solutions did. Specifically, the category-3 high-pH caustic etch solution was the most aggressive resulting in severe general and localized attack after short exposure times in

the 60-120 s range. The low-pH deoxidizer solution also caused general attack and localized pitting corrosion was present after 600 s exposure; however, this solution was much less aggressive than the caustic etch. Pits that were initiated during the pretreatment beyond a threshold critical size on the order of 10 μm significantly increased in size during the subsequent electrochemical anodize process (Fig. 15).

For many design applications (i.e. fracture critical aerospace components), use of caustic etch has been prohibited due to severe pitting corrosion that results. It was established in the present study that machined (wrought) components can be properly anodized without caustic etching if they are relatively free of oils, greases, and oxide scales. In this case, nonetching cleaners are used in conjunction with a nitric-acid based deoxidizer. Although the deoxidizer is not as effective as the caustic etch for activating the surface, the nature of the untreated aluminum's oxide film, being thin (nm scale) and porous, still allows for a reliable anodic film. For commercial applications where the appearance may be most important, or for die forgings and castings, a caustic etch is often necessary to remove oxide scale build-up and contamination particles to achieve a uniform anodic coating. It is important to point out that the low-pH deoxidizer solution also causes localized corrosion; however, not as severely as the caustic etch. With exposure to the deoxidation solution being a required step of the anodize process future quantitative studies using electrochemical measurements are needed to better understand this process.

It is interesting to note that the same microstructural properties such as composition, size, and distribution of constituent particles that influence the corrosion behavior during anodize processing also influence the resistance to fatigue crack initiation as reported in prior investigations (Ref 18, 19). For example, a finer distribution of particles will result in fewer and less severe surface defects that can result in fatigue crack nucleation. In this case, the thermomechanical working history controls the size and distribution of particles, whereas the tighter control limits on impurity elements such as Fe and Si reduces the amount of constituent particles (Ref 20, 21). For highly polished specimens under high-cycle fatigue conditions, Stage-I fatigue can make up the majority of the life until a so-called 'engineering sized crack' is formed (Ref 22). For this discussion, an engineering-sized crack is defined as one that can be detected using standard NDT methods (e.g. dye penetrant), typically on the order of 0.025-0.050 cm (0.010-0.020 in). Future areas of research should be aimed at better understanding the influence of localized corrosion due to pretreatment processing on fatigue behavior.

Acknowledgment

The financial support of Parker Aerospace, Irvine, California, is gratefully acknowledged.

References

1. Military Specification—Mil-A-8625, "Anodic Coatings for Aluminum and Aluminum Alloys," Department of Defense, 25 April 1988
2. ASM International, Corrosion, *Metals Handbook*, Vol. 13, 9th ed., Materials Park, OH, 1987, p 550–552
3. ASM International, Surface Cleaning, Finishing, and Coating, *Metals Handbook*, Vol. 5, 9th ed., Materials Park, OH, 1987, p 571–610
4. S. Wernick, R. Pinner, and P.G. Sheasby, *The Surface Treatment and Finishing of Aluminum and its Alloys*, Vol. 1, 5th ed., ASM International, Metals Park, OH, 1995
5. E.J. Dolley, B. Lee, and R.P. Wei, The Effect of Pitting Corrosion on Fatigue Life, *Fatigue Fract. Eng. Mater. Struct.*, 2000, **23**, p 555–560
6. P.S. Pao, S.J. Gill, and C.R. Feng, On Fatigue Crack Initiation from Corrosion Pits in 7075-T7351 Aluminum Alloy, *Scripta Mater.*, 1998, **43**(5), p 391–396
7. E.E. Stansbury and R.A. Buchanan, *Fundamentals of Electrochemical Corrosion*, ASM International, 2002
8. G.S. Frankel, Pitting Corrosion of Metals—A Summary of Critical Factors, *J. Appl. Electrochem.*, 1998, **145**, p 2186
9. R.P. Wei, C. Liao, and G. Gao, A Transmission Electron Microscopy Study of Constituent-Particle-Induced Corrosion in 7075-T6 and 2024-T3 Aluminum Alloys, *Metal. Mater. Trans. A*, 1998, **29A**, p 1153–1160
10. G.S. Frankel, *Localized Corrosion of Metals; Review of the Rate-Controlling Factors in Initiation and Growth*, Passivity-8, Jasper, Canada, Keynote Address, May 1999
11. N. Birbillis and R.G. Buchheit, Electrochemical Characteristics of Intermetallic Phases in Aluminum Alloys, *J. Electrochem. Soc.*, 2005, **152**(4), p B140–B151
12. R.G. Buchheit, A Compilation of Corrosion Potentials Reported for Intermetallic Phases in Aluminum Alloys, *J. Electrochem. Soc.*, 1995, **142**(11), p 3994–3996
13. Brulin 815D Detergent Product Data Sheet, Brulin Corporation, Indianapolis, IN 46205, USA, 2003
14. Diversey-909 Alkaline Cleaner Product Data Sheet, Diversey Corporation, Livonia, MI, 48150, USA, 2001
15. Oakite 160 Chelated Alkaline Cleaner Product Data Sheet, Chemetall Oakite Corporation, New Providence, NJ 07974, USA, 1992
16. Oakite LNC Liquid Non-Chromated Deoxidizer Product Data Sheet, Chemetall Oakite Corporation, New Providence, NJ 07974, USA, 1992
17. AMS-A-22771, *Aluminum Alloy Forgings, Heat Treated*, SAE International, 1999
18. T.P. Savas and J.C. Earthman, Fatigue and Stress Analysis of a Novel Test Coupon Geometry Developed for Hydraulic Pressure Impulse Cycling, *JTEVA*, 2000, **28**, p 359–366
19. P.E. Magnusen, R.J. Bucci, A.J. Hinkle, and J.L. Rudd, *Fatigue Durability Improvement in Thick Section Metallic Airframe Parts*, White Paper, ALCOA Technical Center, August 1992
20. P.E. Magnusen, R.J. Bucci, A.J. Hinkle, R.L. Rolf, The Influence of Material Quality on Airframe Structural Durability, *7th International Conference on Fracture*, March 20–24, Houston, TX, 1995
21. P.E. Magnusen, R.J. Bucci, A.J. Hinkle, J.R. Brockenbrough, S.M. Miyasato, and H.J. Konish, "Final Report: The Role of Microstructure on the Fatigue Durability of Aluminum Aircraft Alloys," ONR Contract #N00014-91-C-0128. Alcoa Technical Center, Pennsylvania, November 1995
22. R.J. Bucci, R.W. Bush, A.J. Hinkle, H.J. Konish, M. Kulak, R.H. Wygonik, G.W. Kuhlman, and E.D. Seaton, "Property/Performance Attributes of Forgings" *AeroMat'95, ASM International's 6th Advanced Aerospace Materials & Processes Conference*, Anaheim, CA, May 8–11, 1995